# A Statistical Comparison of Meteorological Data Types Derived from Deep Space Network Water Vapor Radiometers

**David D. Morabito,* Stephen Keihm,† and Stephen Slobin‡**

ABSTRACT. — Water vapor radiometers measure the sky brightness along a path through the atmosphere. This sky brightness is a combination of the atmospheric "noise" temperature and the cosmic background. By removing the cosmic contribution, the remaining atmospheric noise temperature contribution can be used to infer atmospheric attenuation and atmospheric noise temperature used in telecommunications link budgets. Water vapor radiometer (WVR) data also have been used to calibrate or experimentally characterize atmospheric error sources in phase data gathered from radio science and very long baseline interferometry (VLBI) experiments. A previous article reported on the comparison of atmospheric attenuation derived from WVR data with that estimated from International Telecommunication Union (ITU) models for the three Deep Space Network (DSN) sites. The focus of this current article is to examine and cross-compare the statistics of the meteorological data types (integrated precipitable water vapor, integrated liquid water content, and wet path delay) extracted from the WVR measurements for all three DSN sites. In this article, we will also compare some of the statistical estimates against those available using ITU models and prediction methods.

## I. Introduction

Water vapor radiometers (WVRs) measure the sky brightness along a path through the atmosphere. Algorithms and calibration procedures have been incorporated to accurately measure this quantity. By removing the cosmic contribution, the remaining atmospheric noise temperature contribution can be used to infer atmospheric attenuation and system noise temperature increase used in telecommunications link budgets. Such statistics on atmospheric attenuation and atmospheric noise temperature contributions for the three Deep Space Network (DSN) sites of Goldstone, California; Madrid, Spain; and Canberra, Austra-

* Communications Architectures and Research Section.
† Instrument Systems Implementation and Concepts Section, retired.
‡ Communications Ground Systems Section.

The research described in this publication was carried out by the Jet Propulsion Laboratory, California Institute of Technology, under a contract with the National Aeronautics and Space Administration. 

lia, are published in the *DSN Telecommunications Link Design Handbook* [1] and periodically updated as more years of data become available.

By sampling multiple frequencies along or near the 22-GHz water absorption line, additional quantities can be extracted from WVR sky brightness measurements. These include integrated precipitable water vapor, integrated liquid water content, and water vapor induced-path delay. Statistical inversion was employed to extract the water vapor products and liquid water content from the multifrequency brightness temperature measurements [2]. Such techniques include comparison of the radiometer estimates with measurements from radiosonde launches in the same locality or at least in a nearby proxy locality.

WVR data have been used to calibrate or experimentally characterize atmospheric error sources in phase data gathered from radio science experiments [3] and very long baseline interferometry (VLBI) experiments [4]. Simultaneous VLBI and WVR experimental measurements on a 21-km baseline within the DSN's Goldstone, California, tracking site demonstrated that WVRs removed a sizable contribution of tropospheric delay fluctuations from the VLBI data [4]. A good review article on the extraction of path delay from microwave radiometry can be found elsewhere in the literature [5].

The differenced path delay between the two spatially separated WVR units forms an additional data type whose statistics provide a measure of atmospheric decorrelation over the spatial distance that can be used in arraying applications. Such statistics are routinely acquired by site test interferometers (STIs) at the DSN sites [6]. In August 2008, two water vapor radiometers were deployed next to each antenna element of an STI in Goldstone, California, in order to validate the atmospheric nature of these measurements [7]. This study found that the fluctuations measured by the WVR baseline were consistent with those measured by the STI, thus providing an added degree of validation.

A previous article [8] provided details on a comparison of calculated atmospheric effects using different methods for the DSN and two Near Earth Network (NEN) sites that are commonly used in telecommunications links. Atmospheric attenuation estimated from International Telecommunication Union (ITU) models was compared against atmospheric attenuation derived from WVR measurements at the three DSN sites and found to be in reasonable agreement. A few discrepancies were believed to be consistent with higher uncertainties in the ITU models or their inputs, especially with the liquid content models (rain and clouds) at higher percentiles. In previous years, this was not as important for NEN sites that typically operated with high margins and given the conservative nature of the ITU rain model estimates. However, with the advent of higher data rates and lower margins in near-Earth communications links, it becomes more important to better characterize the performance of ITU models and identify any improvements that can be made. The DSN attenuation statistics derived from WVRs provided a good testbed in which to cross-compare against the statistics of atmospheric losses derived from ITU prediction methods.

The focus of this article will be to examine and cross-compare the statistics of the integrated precipitable water vapor, integrated liquid water content (such as cloud droplets) and path delay extracted from the multifrequency WVR sky brightness measurements for the DSN

sites. We will also compare these statistical estimates against those using available ITU models and other sources.

## II. The WVR Observations

Data files of integrated water vapor, integrated liquid, and path delay as well as the brightness temperatures at each WVR frequency band were prepared using available advanced WVR (AWVR) data acquired at Goldstone and Madrid, and R6 WVR data acquired at Canberra, Australia. These files also include time tags of year, month, day, hour, minute, and seconds. Figure 1 displays a photo of the AWVR residing near the 34-m-diameter beam-waveguide antenna DSS-25 at the Apollo site in Goldstone, California.

The time series for Goldstone and Madrid AWVR results include the three brightness temperatures (in K) at 22.2 GHz, 23.8 GHz, and 31.4 GHz, wet path delay (PD in cm), integrated vapor (Vz in cm), and cloud liquid burden (Lz in μm) in yearly files. Retrieval algorithms for integrated water vapor (not previously available) were generated based on radiosonde data from Desert Rock, Nevada (which served as a proxy site for Goldstone) and the Madrid weather station. The Madrid site has its own radiosonde launch, which was used in calibration of the Madrid AWVR retrieval algorithms. The Vz algorithm (as also for the PD and Lz algorithms) used only the three-channel AWVR data as input observables. Retrieval coefficients were generated for both sites based on subsets of the radiosonde data corresponding to three parts of the year (November–February; March–July; August–October). Thus, six different sets of retrieval coefficients were used (three "seasons" times two sites).

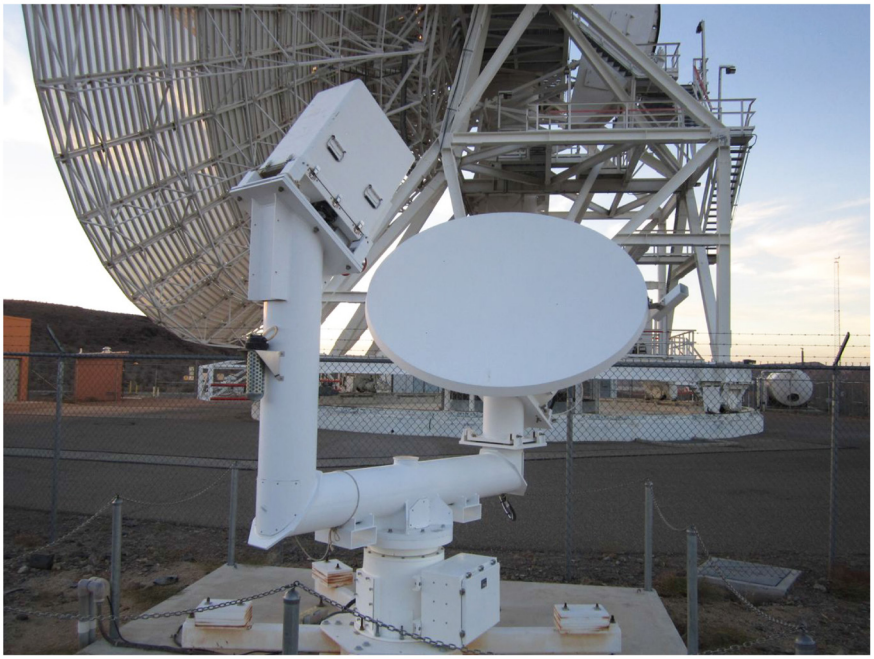

**Figure 1. The advanced water vapor radiometer (AWVR) that resides next to the 34-m-diameter beam-waveguide antenna DSS-25 in the background.**

The output data files for Goldstone extend in time from January 2001 through June 2015 with significant gaps that include August–October, 2006; May 2009; April 2010; August 2012; and January–July 2013. The output data files for Madrid extend in time from February 2006 through December 2014 with some gaps that include September–October 2012.

The files of time-dependent retrieved values of wet path delay (PD in cm), integrated vapor (Vz in cm), and cloud liquid burden (Lz in μm) for Canberra were derived from the R06 WVR unit covering years from 1999 to 2009 (excluding 2000). The R06 unit is an older model WVR that operates at just two frequencies, 20.7 GHz and 31.4 GHz [9]. The brightness temperatures at these two frequencies were also included in the files.

The 31.4-GHz brightness temperature error reflects the difference between the direct zenith measurement and the air mass converted zenith equivalent value derived from the average of the 30 deg elevation measurements obtained during the WVR tip curve sequence. Large values of this error indicate the presence of moisture during rainy conditions, predominately near the top of the R06 unit where the window was more susceptible to accumulation of water when pointed at zenith. The R06 data were filtered to remove error levels that exceeded 3 K and also to remove other clearly non-physical brightness temperature data (for example, values less than 9 K). The statistical algorithms for Vz, PD, and Lz were derived from Canberra radiosonde data.

There were a number of problems associated with the R06 unit in Canberra that led to some large gaps (for example, no data from year 2000) and the eventual shutdown of the unit in 2009. However, it is believed that the filtered data provide a useful chronology of the Canberra water-related atmospheric constituents over the 10-year period, although certainly not as accurate as the Goldstone and Madrid data, which were based on AWVR measurements.

## III. Examination of Total Columnar Water Vapor Statistics

Precipitable water vapor is an important meteorological quantity whose statistics are important in characterizing and understanding weather effects on telecommunications links (such as gaseous attenuation) for the various sites. This will be important in future studies (such as for operational weather forecasting applications) involved in telecommunications link scenarios at higher frequencies (such as at Ka-band 26 GHz, 32 GHz, 40 GHz, and optical). Integrated water vapor is synonymous with "total water vapor content" as described by the ITU [10]. One cm of precipitable water vapor is equivalent to 1 gm/cm$^2$.

The annual statistics of the total water vapor content were examined and compared against those derived from ITU global maps of this quantity [10]. The ITU maps are based on a 40-year average of European Centre for Medium-Range Weather Forecasts (ECMWF) predictions on a 1.125-deg by 1.125-deg grid with bilinear interpolation performed between grid points to the location of the WVR site. Total water vapor content along the zenith path can also be described in terms of integrated vapor or precipitable water vapor. For most of this study, integrated water vapor data were removed from calculation of statistics whenever the corresponding liquid water content exceeded 500 μm due to diminished accuracy of the algorithm in estimating water vapor content under these conditions.

Figure 2 displays the cumulative distribution curves of zenith precipitable water vapor (Vz) for Goldstone for each year of data (color curves) along with that derived from the ITU model (black curve). The statistics are summarized in Table 1 for Goldstone's precipitable water vapor. We see that there is about 1 cm of precipitable water vapor on average typically present at Goldstone reaching values as high as 5.8 cm and as low as 0.1 cm. The average of the 15 yearly medians (50 percent cumulative distribution column) obtained from the AWVR is 0.83 ±0.06 cm, which lies below the ITU median value of 1.09 cm.

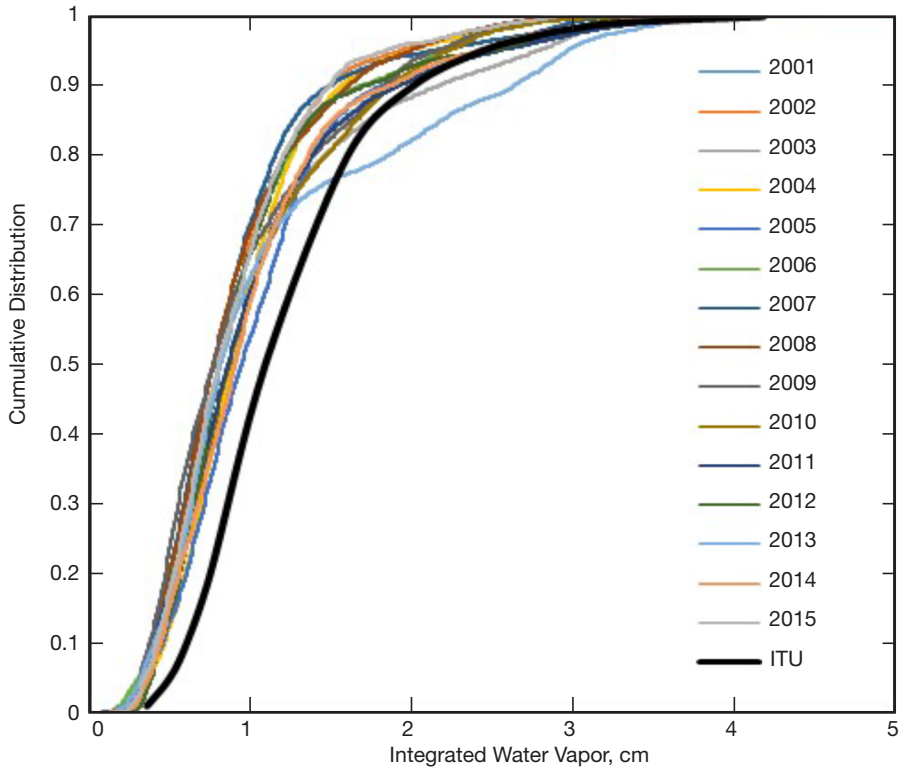


**Figure 2. Cumulative distribution curves of integrated water vapor derived from Goldstone AWVR data along with that derived from ITU Global Maps.**

The curve for 2013 in Figure 2 (light blue) deviates greatly from the group of other AWVR precipitable water vapor distribution curves at the higher cumulative distributions. Since this curve is based on good calibrated data, we assume it is real. It should be pointed out that the 2013 data excludes records from January 1 to July 25 due to various calibration issues. To further evaluate the 2013 anomaly, we examined the surface meteorological data acquired at the nearby weather station. The relative humidity statistics for 2013 did not show any significant differences for 2013 with that of adjacent years (even if the January–July data were removed for 2013). A closer examination of the time series of the Goldstone 2013 integrated water vapor accounted for the unusual shape of the 2013 curve in Figure 2. This was due to a very humid summer followed by relatively dry autumn and winter months over the partial year period.

The cumulative distribution curve derived from ITU global maps of integrated water vapor [10] is also plotted in Figure 2 (thick black curve). The ITU curve is based on data whose temporal range does not overlap with that of the AWVR data sets. The distribution

**Table 1. Goldstone AWVR precipitable water vapor statistics.**

| Year | Number of Data Points | Average, cm | Minimum, cm | Maximum, cm | 50% CD, cm | 90% CD, cm | 99% CD, cm | 99.9% CD, cm |
|---|---|---|---|---|---|---|---|---|
| 2001 | 85434 | 0.89 | 0.07 | 5.78 | 0.76 | 1.60 | 2.61 | 3.04 |
| 2002 | 87106 | 0.92 | 0.12 | 3.53 | 0.80 | 1.48 | 2.60 | 3.16 |
| 2003 | 88478 | 1.08 | 0.07 | 3.75 | 0.89 | 2.17 | 3.25 | 3.55 |
| 2004 | 93322 | 0.97 | 0.11 | 3.69 | 0.87 | 1.56 | 2.70 | 3.18 |
| 2005 | 85554 | 1.07 | 0.13 | 4.00 | 0.94 | 1.81 | 3.19 | 3.81 |
| 2006 | 72960 | 0.93 | 0.11 | 3.35 | 0.81 | 1.68 | 2.69 | 3.13 |
| 2007 | 85890 | 0.89 | 0.12 | 3.61 | 0.76 | 1.49 | 2.99 | 3.41 |
| 2008 | 85434 | 0.89 | 0.07 | 5.78 | 0.76 | 1.60 | 2.61 | 3.04 |
| 2009 | 76341 | 0.94 | 0.09 | 3.47 | 0.77 | 1.83 | 2.73 | 3.15 |
| 2010 | 73344 | 1.02 | 0.08 | 4.38 | 0.86 | 1.87 | 2.77 | 3.25 |
| 2011 | 87203 | 1.03 | 0.08 | 3.98 | 0.85 | 1.92 | 3.44 | 3.76 |
| 2012 | 63122 | 0.98 | 0.20 | 3.68 | 0.81 | 1.72 | 3.14 | 3.46 |
| 2013 | 43110 | 1.14 | 0.11 | 3.97 | 0.81 | 2.63 | 3.59 | 3.91 |
| 2014 | 99746 | 1.03 | 0.12 | 3.86 | 0.90 | 1.86 | 3.19 | 3.51 |
| 2015 | 48650 | 0.90 | 0.16 | 2.96 | 0.80 | 1.48 | 2.65 | 2.90 |
| Overall | 1175694 | 0.98 | 0.07 | 5.78 | 0.83 | 1.78 | 2.94 | 3.35 |
| ITU | — | — | — | — | 1.09 | 2.01 | 3.28 | 4.18 |

of the ITU global map values of this quantity were interpolated to refer to the latitude and longitude of DSS-25 (which resides next to the Goldstone AWVR). The ITU curve displays a wetter situation as compared to the AWVR values, at least for cumulative distributions up to about 85 percent. The curve then "merges" within the AWVR curves at distributions above 85 percent, consistent with the results from an earlier study [8] involving atmospheric attenuation derived from WVR/AWVR data displayed in the 810-005 tables [1] and ITU models and maps.

Figure 3 displays the cumulative distributions of the Madrid AWVR precipitable water vapor measurements (color curves) and that derived from ITU global map values (thick black curve). The ITU global map distribution of integrated water vapor for Madrid is in agreement with the AWVR-derived results, as shown in Figure 3, unlike that of Goldstone (Figure 2). The heavy black curve of the ITU global map distribution of integrated water vapor for Madrid "slashes" right through most of the AWVR single-year distribution curves. Only the Madrid 2012 curve appears to be offset to the left of the cluster of all other AWVR curves. It should be pointed out that the 2012 distribution curve (blue) was the only year in which there existed a significant data gap (September–October 2012). The average of the Madrid Vz from Table 2 (filtered for high liquid content) is about 1.35 cm, which is somewhat greater than the ~1 cm average for Goldstone. The 90 percent values are also of comparable proportional magnitudes; 1.8 cm for Goldstone versus 2.1 cm for Madrid. However, the yearly maximums for Madrid range from 3.2 to 3.9 cm, which is a smaller range than that for Goldstone (3.0 to 5.8 cm). This difference could be attributed to the fact that the higher temperatures encountered in the Goldstone summer climate allow for higher vapor content. The average of the yearly medians extracted from the AWVR data is 1.32 ±0.09 cm, which is in very good agreement with the ITU median value of 1.31 cm.

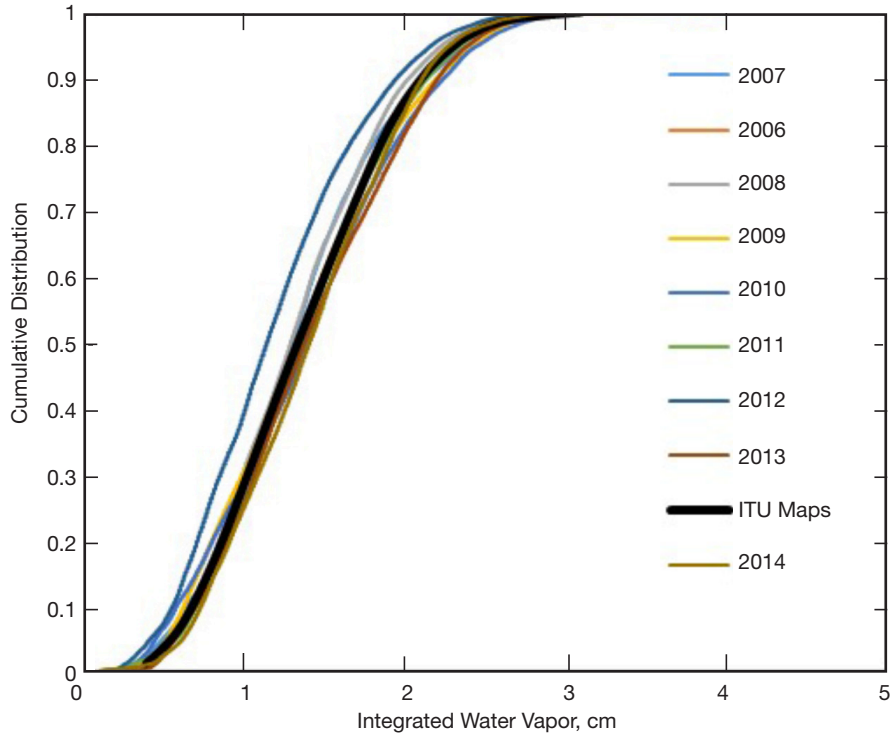


**Figure 3. Cumulative distribution curves of integrated water vapor derived from Madrid AWVR data along with that derived from ITU Global Map values of that quantity.**

**Table 2. Madrid AWVR precipitable water vapor statistics.**

| Year | Number of Data Points | Average, cm | Minimum, cm | Maximum, cm | 50% CD, cm | 90% CD, cm | 99% CD, cm | 99.9% CD, cm |
|---|---|---|---|---|---|---|---|---|
| 2006 | 86411 | 1.46 | 0.16 | 3.50 | 1.44 | 2.28 | 2.73 | 3.06 |
| 2007 | 93735 | 1.32 | 0.16 | 3.79 | 1.28 | 2.12 | 2.74 | 3.08 |
| 2008 | 81302 | 1.30 | 0.12 | 3.34 | 1.26 | 2.00 | 2.59 | 2.98 |
| 2009 | 96562 | 1.34 | 0.16 | 3.35 | 1.30 | 2.18 | 2.74 | 3.00 |
| 2010 | 94414 | 1.38 | 0.11 | 3.86 | 1.37 | 2.22 | 2.82 | 3.35 |
| 2011 | 88384 | 1.37 | 0.09 | 3.40 | 1.34 | 2.12 | 2.61 | 2.93 |
| 2012 | 76339 | 1.17 | 0.11 | 3.25 | 1.12 | 1.93 | 2.53 | 2.90 |
| 2013 | 75418 | 1.41 | 0.15 | 3.74 | 1.35 | 2.19 | 2.77 | 3.43 |
| 2014 | 81059 | 1.39 | 0.07 | 3.15 | 1.38 | 2.09 | 2.64 | 2.95 |
| Overall | 773624 | 1.35 | 0.07 | 3.86 | 1.32 | 2.13 | 2.69 | 3.08 |
| ITU | — | — | — | — | 1.31 | 2.08 | 2.68 | 3.07 |

The ITU global map distribution of integrated water vapor for Canberra is also in good agreement with the WVR-derived results, as shown in Figure 4. The heavy black curve of the ITU global map distribution of integrated water vapor for Canberra "slashes" through most of the WVR single-year distribution curves. Only the 2009 curve appears to be somewhat of an outlier, lying further to the right of the other curves; however, the data for 2009 are only a fraction of the year as inferred from Table 3 ("Number of Data Points" column). The Canberra integrated water vapor statistics have been filtered to remove points when liquid water content exceeded 500 μm. If we remove the 2009 curve, the agreement of the ITU model with the remainder of the Canberra curves is excellent. The average of the yearly median values for Canberra is 1.38 ±0.17 cm, which is in good agreement with the ITU median value of 1.33 cm.

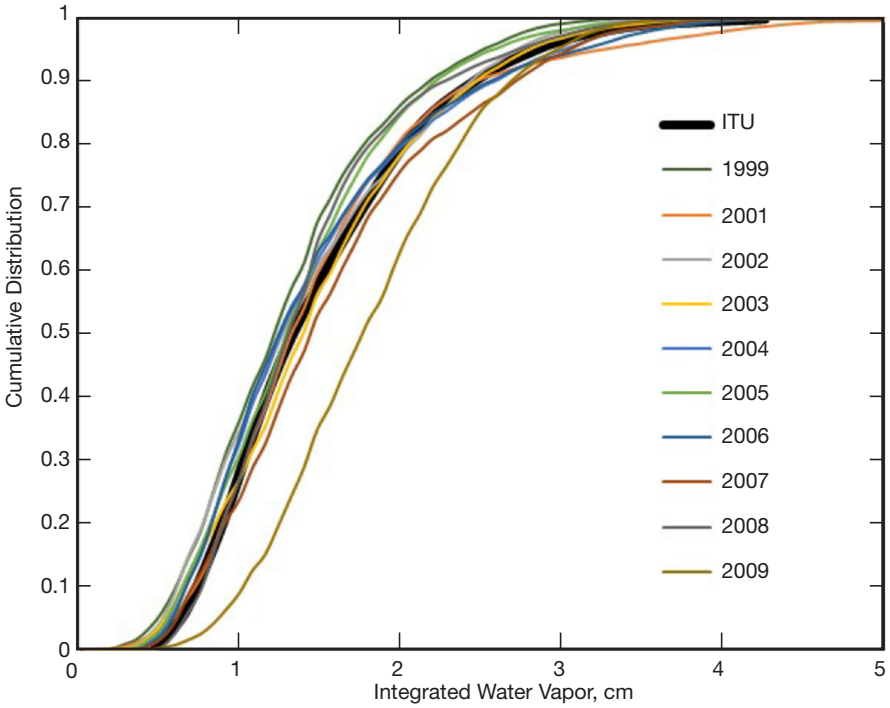


**Figure 4. Cumulative distribution curves of integrated water vapor derived from Canberra WVR data along with that derived from ITU global map values of that quantity.**

Thus, we have excellent agreement between the distribution curves derived from Madrid AWVR and Canberra WVR data with those derived from the respective ITU global map curves of the integrated water vapor. The ITU global map values for the Madrid area may have been based on significantly more local data than those for the Goldstone site. The Madrid area also has a nearby operational radiosonde. The Madrid radiosonde co-location and large amount of data in the ITU data banks thus perhaps explain the better agreement between the ITU and AWVR statistics at Madrid relative to those at the Goldstone site.

Figure 5 (Figure 1 of [8], reproduced here) shows that the surface water vapor density from the ITU global maps is consistent with that derived from the surface meteorological data from the Madrid site (blue solid and dashed curves lie on top of each other), whereas the

**Table 3. Canberra WVR precipitable water vapor statistics.**

| Year | Number of Data Points | Average, cm | Minimum, cm | Maximum, cm | 50% CD, cm | 90% CD, cm | 99% CD, cm | 99.9% CD, cm |
|---|---|---|---|---|---|---|---|---|
| 1999 | 51066 | 1.34 | 0.12 | 3.76 | 1.25 | 2.22 | 3.00 | 3.37 |
| 2001 | 60407 | 1.55 | 0.10 | 6.72 | 1.35 | 2.50 | 4.43 | 5.97 |
| 2002 | 102435 | 1.44 | 0.16 | 5.17 | 1.30 | 2.47 | 3.24 | 3.65 |
| 2003 | 97444 | 1.52 | 0.21 | 4.86 | 1.42 | 2.50 | 3.48 | 4.12 |
| 2004 | 77362 | 1.48 | 0.23 | 4.82 | 1.28 | 2.60 | 3.75 | 4.27 |
| 2005 | 69445 | 1.41 | 0.23 | 5.17 | 1.33 | 2.25 | 3.30 | 4.20 |
| 2006 | 102865 | 1.48 | 0.21 | 5.40 | 1.26 | 2.59 | 3.86 | 4.40 |
| 2007 | 67418 | 1.61 | 0.28 | 6.79 | 1.47 | 2.74 | 3.70 | 4.12 |
| 2008 | 43725 | 1.45 | 0.38 | 4.54 | 1.33 | 2.30 | 3.37 | 3.97 |
| 2009 | 21409 | 1.85 | 0.30 | 4.65 | 1.81 | 2.72 | 3.38 | 3.79 |
| Overall | 693576 | 1.51 | 0.10 | 6.79 | 1.38 | 2.49 | 3.55 | 4.19 |
| ITU | — | — | — | — | 1.33 | 2.46 | 3.57 | 4.26 |

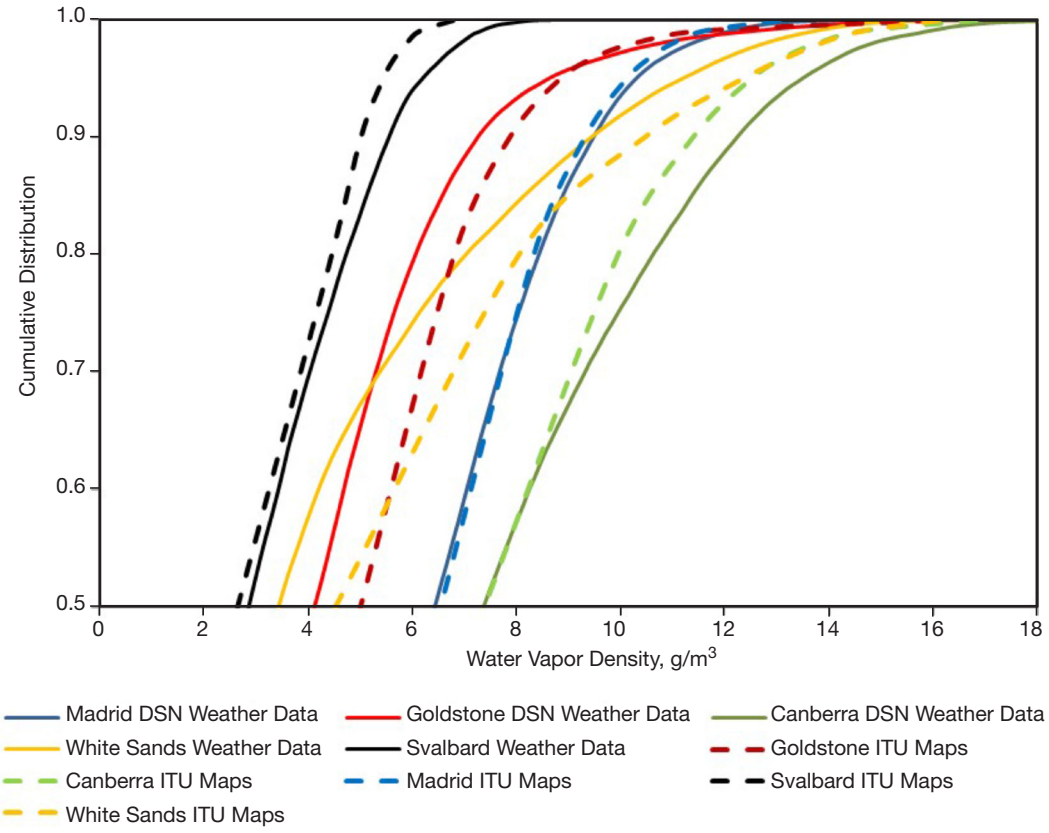


**Figure 5. Cumulative distribution of surface water vapor density for different sites extracted from several years of surface weather data (solid curves) and ITU global map values (dashed curves). Taken from Figure 1 in [8].**

AWVR integrated water vapor was consistent with the ITU integrated water vapor (see Figure 3). The surface water vapor density for Canberra (green curves in Figure 5) compares roughly with the integrated water vapor ITU and annual WVR curves (see Figure 4). The Goldstone ITU-derived integrated water vapor curve lies at a higher value than that of the AWVR derived curve for a given percentile below ~90 percent (Figure 2), consistent with the surface water vapor density comparison (see Figure 5), where the ITU global map derived curve (dashed red) shows higher values than the distribution calculated from local surface data (solid red) for a given percentile below ~95 percent.

## IV. Examination of Total Columnar Liquid Statistics

Cloud liquid burden is synonymous with total columnar content of reduced cloud liquid as described by the ITU [11]. The units of total liquid columnar content, $kg/m^2$, can be translated to units of μm by dividing by the liquid water density of 1 $gm/cm^3$ and performing the necessary conversions. Thus, 1 $kg/m^2$ translates to 1 mm (or 1000 μm) of liquid water.

The liquid water content estimates extracted from the WVRs were statistically characterized and the results are summarized in Figure 6 and Table 4 for Goldstone, Figure 7 and Table 5 for Madrid, and Figure 8 and Table 6 for Canberra. We see that the average columnar liquid content runs at about 15.3 ±5.5 μm over 15 years of data for Goldstone, about 67 ±16 μm over 9 years of data for Madrid, and 75 ±15 μm over 9 years of data for Canberra. The curves for Goldstone in Figure 6 show significant percentages where there is zero liquid water content (evident from the elevated intersections of the curves on the y-axis). For most years, the liquid content is zero for over 50 percent of the time consistent with the dry desert climate of Goldstone. The curves for Madrid (Figure 7) and Canberra (Figure 8) tend to intersect the y-axis at lower percentages, with Canberra having the lowest intersection values. This is consistent with Goldstone being the driest and Canberra being the wettest of the three DSN sites. Characterizing the liquid water content statistics at the three DSN sites will be important as weather forecasting techniques are developed for the purpose of optimizing data return for Ka-band operations.

A first-order comparison of the ITU statistics of cloud liquid burden using the procedures outlined in [11] were found to be roughly comparable to the statistics determined from the WVR measurements as documented in this article. The observed discrepancies can be attributed to the facts that the data sets used to estimate the statistics do not overlap, and are of different lengths. This is not surprising given the highly variable climatic year-to-year variation of cloud liquid.

In all cases, the minimum liquid content reaches 0 μm for some (Canberra) to significant (Goldstone) periods of time. The maximum liquid content can reach or exceed values of 6000 μm (0.6 cm) during heavy saturated conditions. Liquid water is not significant in contributing to path delay (discussed next), but its large and highly variable effects on noise temperature complicate the accurate determination of path delay.

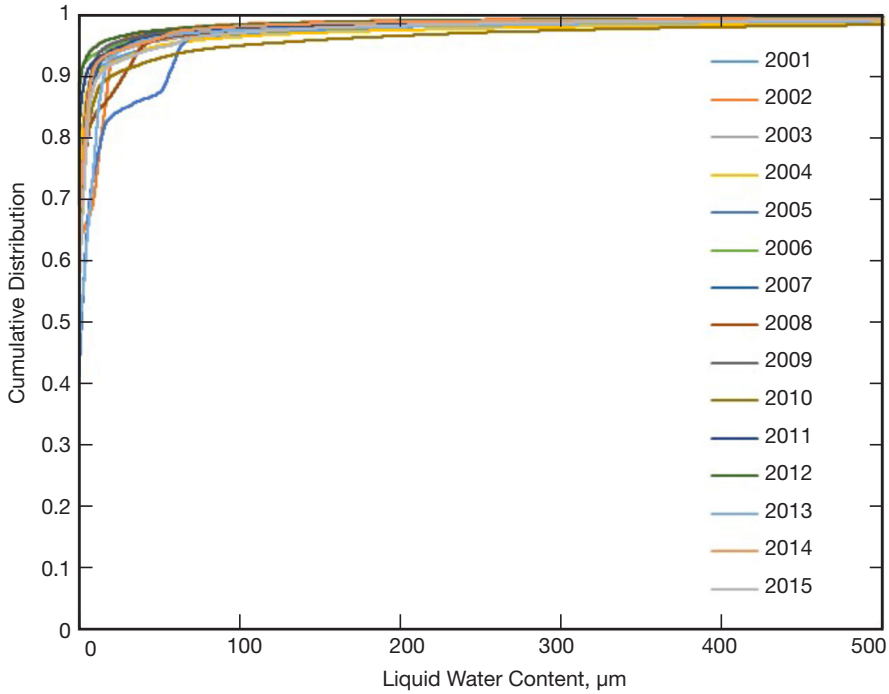


**Figure 6. Cumulative distribution of liquid water content for Goldstone.**

**Table 4. Liquid water content statistics, Goldstone AWVR.**

| Year | Number of Data Points | Average, µm | Minimum, µm | Maximum, µm | 50%, µm | 90%, µm | 99%, µm | 99.9%, µm |
|---|---|---|---|---|---|---|---|---|
| 2001 | 95375 | 13.35 | 0.0 | 2758.8 | 0.0 | 8.8 | 338.2 | 1116.3 |
| 2002 | 87346 | 11.15 | 0.0 | 3316.6 | 0.0 | 19.0 | 153.7 | 945.5 |
| 2003 | 88962 | 13.31 | 0.0 | 5949.2 | 0.0 | 8.9 | 308.9 | 1486.6 |
| 2004 | 94411 | 23.03 | 0.0 | 3423.4 | 0.0 | 9.5 | 564.7 | 3239.5 |
| 2005 | 86039 | 19.92 | 0.0 | 3374.2 | 2.1 | 55.9 | 265.1 | 1522.3 |
| 2006 | 73392 | 14.57 | 0.0 | 3234.8 | 0.0 | 0.2 | 287.9 | 2981.4 |
| 2007 | 86292 | 13.09 | 0.0 | 3359.5 | 0.0 | 10.5 | 197.2 | 2608.9 |
| 2008 | 85995 | 19.71 | 0.0 | 3419.1 | 0.0 | 27.8 | 291.4 | 3287.8 |
| 2009 | 76588 | 8.75 | 0.0 | 3275.9 | 0.0 | 7.8 | 199.8 | 819.1 |
| 2010 | 74445 | 28.52 | 0.0 | 3519.1 | 0.0 | 19.7 | 691.0 | 2462.0 |
| 2011 | 87609 | 13.24 | 0.0 | 3373.1 | 0.0 | 4.6 | 232.9 | 3097.2 |
| 2012 | 63325 | 6.93 | 0.0 | 2570.6 | 0.0 | 1.6 | 170.5 | 927.3 |
| 2013 | 43481 | 16.86 | 0.0 | 2432.8 | 1.4 | 15.8 | 420.6 | 1199.7 |
| 2014 | 100178 | 10.96 | 0.0 | 3440.4 | 0.0 | 8.5 | 210.6 | 1302.0 |
| 2015 | 49013 | 16.11 | 0.0 | 2179.7 | 0.0 | 12.4 | 340.8 | 1464.2 |
| Overall | 1192451 | 15.30 | 0.0 | 5949.2 | 0.2 | 14.1 | 311.6 | 1897.3 |

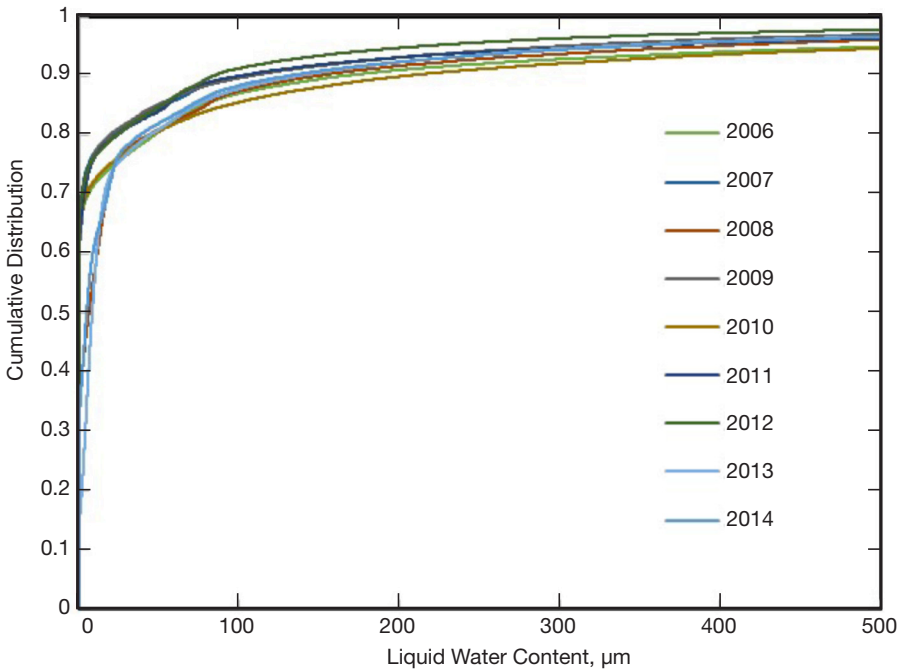


**Figure 7. Cumulative distribution of liquid water content for Madrid.**

**Table 5. Liquid water content statistics, Madrid AWVR.**

| Year | Number of Data Points | Average, µm | Minimum, µm | Maximum, µm | 50%, µm | 90%, µm | 99%, µm | 99.9%, µm |
|---|---|---|---|---|---|---|---|---|
| 2006 | 90867 | 95.60 | 0.0 | 4310.1 | 0.0 | 159.7 | 1999.7 | 4050.2 |
| 2007 | 96714 | 56.89 | 0.0 | 4144.0 | 0.0 | 102.3 | 1148.9 | 3000.5 |
| 2008 | 84441 | 68.82 | 0.0 | 3866.8 | 5.6 | 143.6 | 1167.8 | 2656.2 |
| 2009 | 99337 | 58.06 | 0.0 | 4089.3 | 0.0 | 103.3 | 1105.7 | 3905.3 |
| 2010 | 99610 | 86.18 | 0.0 | 4152.3 | 0.0 | 197.6 | 1509.5 | 3364.2 |
| 2011 | 91495 | 60.64 | 0.0 | 3812.5 | 0.0 | 96.4 | 1250.0 | 3310.9 |
| 2012 | 77919 | 42.82 | 0.0 | 6500.8 | 0.0 | 82.1 | 802.3 | 2385.6 |
| 2013 | 77884 | 70.56 | 0.0 | 4002.5 | 7.7 | 133.4 | 1287.3 | 3507.3 |
| 2014 | 83747 | 63.79 | 0.0 | 4026.8 | 4.3 | 126.4 | 1151.0 | 2825.9 |
| Overall | 802014 | 67.04 | 0.0 | 6500.8 | 1.96 | 127.2 | 1269.1 | 3222.9 |

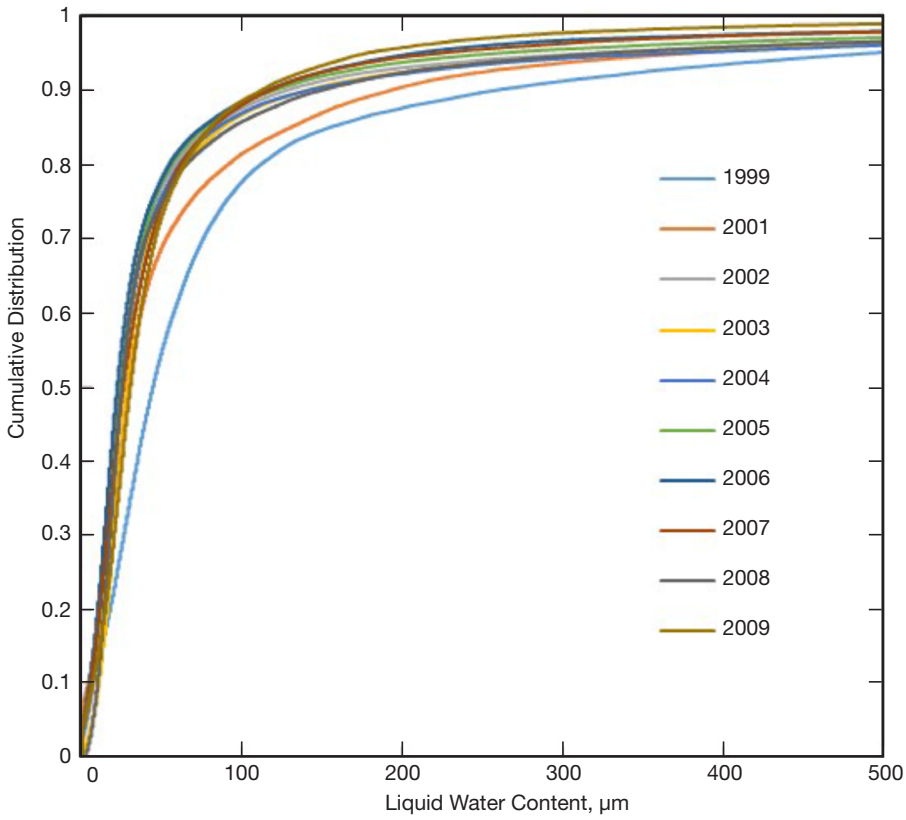


**Figure 8. Cumulative distribution of liquid water content for Canberra.**

**Table 6. Liquid water content statistics, Canberra WVR.**

| Year | Number of Data Points | Average, µm | Minimum, µm | Maximum, µm | 50%, µm | 90%, µm | 99%, µm | 99.9%, µm |
|---|---|---|---|---|---|---|---|---|
| 1999 | 53578 | 105.82 | 0.0 | 2631.0 | 44.0 | 259.0 | 1141.0 | 2001.0 |
| 2001 | 62649 | 84.52 | 0.0 | 2753.0 | 29.0 | 193.0 | 1065.0 | 2148.0 |
| 2002 | 105980 | 73.80 | 0.0 | 2715.0 | 25.0 | 128.0 | 1087.0 | 2136.0 |
| 2003 | 101213 | 81.10 | 0.0 | 2680.0 | 28.0 | 141.0 | 1202.0 | 2251.0 |
| 2004 | 80420 | 80.98 | 0.0 | 2725.0 | 24.0 | 142.0 | 1272.0 | 2375.0 |
| 2005 | 71463 | 68.69 | 0.0 | 2704.0 | 24.0 | 120.0 | 1127.0 | 1965.0 |
| 2006 | 105009 | 58.30 | 0.0 | 2688.0 | 22.0 | 116.0 | 819.0 | 1816.0 |
| 2007 | 68858 | 64.85 | 0.0 | 2736.0 | 26.0 | 118.0 | 905.0 | 2134.0 |
| 2008 | 45241 | 77.26 | 0.0 | 2670.0 | 25.0 | 150.0 | 1127.0 | 2023.0 |
| 2009 | 21637 | 56.44 | 0.0 | 2618.0 | 30.0 | 112.0 | 527.0 | 1504.0 |
| Overall | 716048 | 75.18 | 0.0 | 2753.0 | 27.7 | 147.9 | 1027.2 | 2035.3 |

## V. Examination of Zenith Wet Path Delay Statistics

The sampling of brightness temperature at different frequencies about the 22-GHz water absorption line can also be used to estimate wet path delay using appropriate calibration techniques and algorithms. Such information is important for radio science and navigation error budgets, where calibration is routinely employed to remove both dry and wet path delay contributions from radiometric data types. The wet path delay cumulative distributions and statistics derived from the DSN WVR data are shown in Figure 9 and Table 7 for Goldstone, Figure 10 and Table 8 for Madrid, and Figure 11 and Table 9 for Canberra. Here we see the path delays for the wetter Madrid and Canberra climates tend to be greater than that of the drier Goldstone climate for a given percentile.

ITU global maps of wet path delay cumulative distributions were not readily available for comparison. Thus, instead we compared average values of path delay between the WVR and ITU methods. The average path delay value of 6.26 cm (over a million records) for Goldstone (see Table 7) is in good agreement with measured annual mean values of 6.42 cm from previous work [12], and a value of 6.12 cm derived from an ITU path delay model.[1] The minimum path delay for Goldstone was recorded at 0.61 cm, while the maximum value is 37.56 cm (see Table 7). The range in values of zenith path delay shown in Figure 9 and Table 7 for Goldstone are consistent with the range of values determined from early radiosonde measurements for the semi-arid locations in California [14].

For Madrid, the average AWVR path delay value of 8.63 cm from Table 8 lies much higher than the ITU average of 7.13 cm,[2] although the ITU average does lie close to the lower end of the year-to-year averages for Madrid that range from 7.53 cm to 9.32 cm. The minimum zenith path delay for Madrid is 0.5 cm and the maximum is about 26 cm.

For Canberra, the average path delay value of 9.58 cm from Table 9 lies much higher than the 7.33 cm average ITU value.[3] The year-to-year averages for Canberra wet zenith path delay range from 8.53 cm to 11.54 cm. The minimum path delay for Canberra is about 1 cm and the maximum path delay is 42.1 cm. This maximum value at Canberra is comparable to other wet path delay maximums that can reach near 50 cm at other tropical sites.

It is instructive to examine the relationships between the data types and verify these relationships against expectations and previous work. The path delay (PD) versus precipitable water vapor (Vz) data for sample one-year periods are plotted for Goldstone, Madrid, and Canberra in Figures 12, 13, and 14, respectively.

Linear fits of PD versus Vz derived from the WVR data yield the following relationships:

| | |
|---|---|
| *Goldstone* | PD = 6.51 Vz – 0.13 cm |
| *Madrid* | PD = 6.65 Vz – 0.28 cm |
| *Canberra* | PD = 6.00 Vz + 0.54 cm |

[1] H. Berger, personal communication, Northrop-Grumman, September 2015, using the method described in [13].

[2] Ibid.

[3] H. Berger, personal communication, Northrop-Grumman, September 2015.

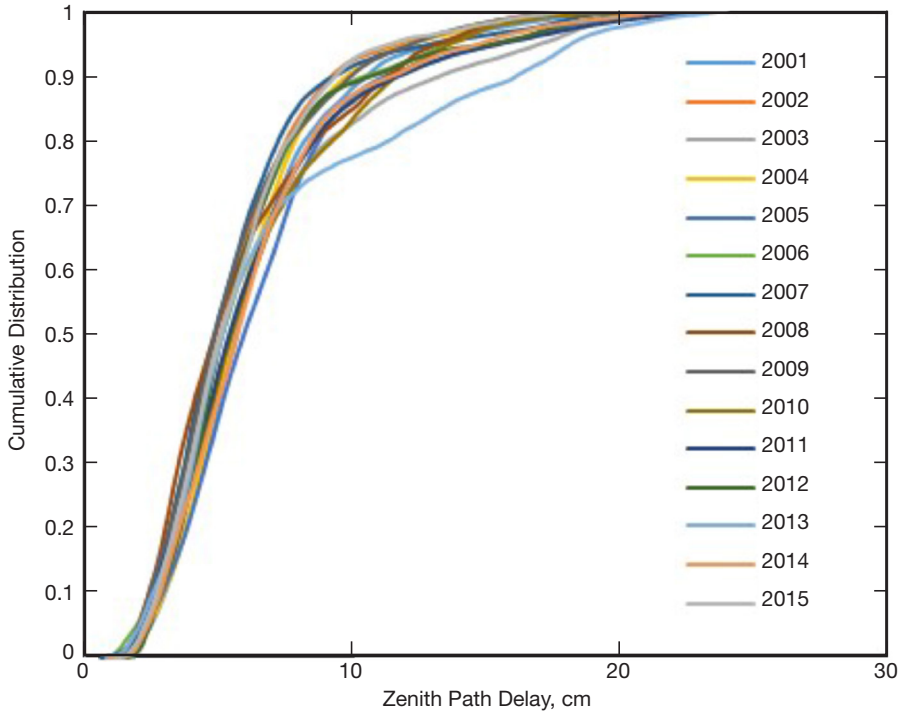


**Figure 9. Cumulative distribution of zenith wet path delay for Goldstone.**

**Table 7. Zenith wet path delay statistics, Goldstone AWVR.**

| Year | Number of Data Points | Average, cm | Minimum, cm | Maximum, cm | 50% CD, cm | 90% CD, cm | 99% CD, cm | 99.9% CD, cm |
|---|---|---|---|---|---|---|---|---|
| 2001 | 94903 | 6.38 | 0.92 | 23.13 | 5.58 | 10.50 | 17.70 | 20.82 |
| 2002 | 87106 | 5.83 | 0.94 | 22.18 | 4.98 | 9.18 | 16.02 | 19.38 |
| 2003 | 88478 | 6.85 | 0.61 | 24.31 | 5.58 | 13.26 | 19.98 | 21.90 |
| 2004 | 93322 | 6.16 | 0.79 | 23.61 | 5.46 | 9.78 | 16.62 | 19.74 |
| 2005 | 85554 | 6.81 | 1.09 | 25.79 | 5.94 | 11.22 | 19.62 | 22.86 |
| 2006 | 72960 | 5.88 | 0.81 | 22.19 | 5.10 | 10.50 | 16.50 | 19.38 |
| 2007 | 85890 | 5.69 | 0.90 | 23.05 | 4.74 | 9.30 | 18.30 | 21.30 |
| 2008 | 85434 | 5.71 | 0.62 | 37.56 | 4.86 | 9.90 | 16.14 | 18.42 |
| 2009 | 76341 | 5.97 | 0.70 | 22.78 | 4.86 | 11.34 | 16.74 | 19.26 |
| 2010 | 73344 | 6.49 | 0.63 | 29.02 | 5.46 | 11.58 | 16.98 | 19.98 |
| 2011 | 87203 | 6.50 | 0.63 | 25.65 | 5.34 | 11.70 | 21.06 | 23.10 |
| 2012 | 63122 | 6.18 | 1.37 | 23.59 | 5.10 | 10.74 | 19.38 | 21.42 |
| 2013 | 43110 | 7.20 | 0.81 | 24.49 | 5.10 | 16.14 | 21.90 | 23.58 |
| 2014 | 99746 | 6.53 | 0.89 | 24.83 | 5.70 | 11.46 | 19.74 | 21.90 |
| 2015 | 48650 | 5.77 | 1.16 | 18.39 | 4.98 | 9.30 | 16.26 | 17.82 |
| Overall | 1185163 | 6.26 | 0.61 | 37.56 | 5.25 | 11.06 | 18.20 | 20.72 |

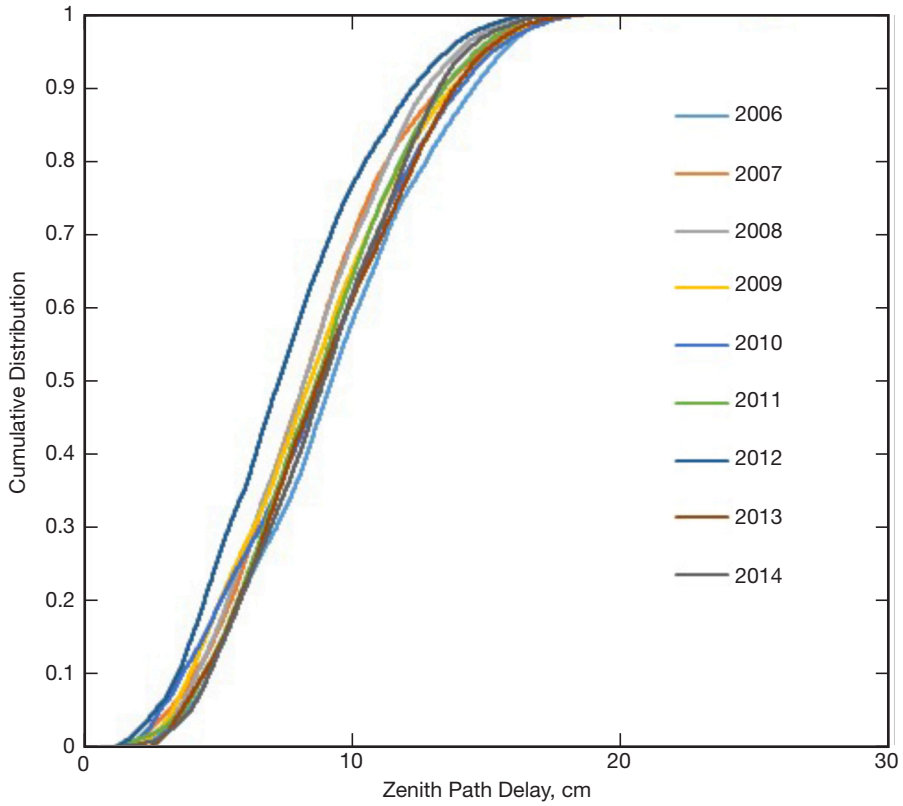


**Figure 10. Cumulative distribution of zenith wet path delay for Madrid.**

**Table 8. Zenith wet path delay statistics, Madrid AWVR.**

| Year | Number of Data Points | Average, cm | Minimum, cm | Maximum, cm | 50% CD, cm | 90% CD, cm | 99% CD, cm | 99.9% CD, cm |
|---|---|---|---|---|---|---|---|---|
| 2006 | 86411 | 9.32 | 1.20 | 23.70 | 9.15 | 14.49 | 17.57 | 20.14 |
| 2007 | 93736 | 8.43 | 1.05 | 25.23 | 8.15 | 13.37 | 17.44 | 19.96 |
| 2008 | 81302 | 8.34 | 0.96 | 22.70 | 8.16 | 12.76 | 16.24 | 19.37 |
| 2009 | 96562 | 8.60 | 1.04 | 22.27 | 8.36 | 13.74 | 17.36 | 19.60 |
| 2010 | 94414 | 8.82 | 0.73 | 26.01 | 8.81 | 14.02 | 17.88 | 21.65 |
| 2011 | 88384 | 8.74 | 0.65 | 23.06 | 8.61 | 13.42 | 16.47 | 18.76 |
| 2012 | 76339 | 7.53 | 0.75 | 22.04 | 7.20 | 12.28 | 15.97 | 18.51 |
| 2013 | 75418 | 9.01 | 0.98 | 25.01 | 8.70 | 13.80 | 17.62 | 22.16 |
| 2014 | 81059 | 8.92 | 0.51 | 21.23 | 8.86 | 13.20 | 16.79 | 18.95 |
| Overall | 773625 | 8.63 | 0.51 | 26.01 | 8.44 | 13.45 | 17.04 | 19.90 |

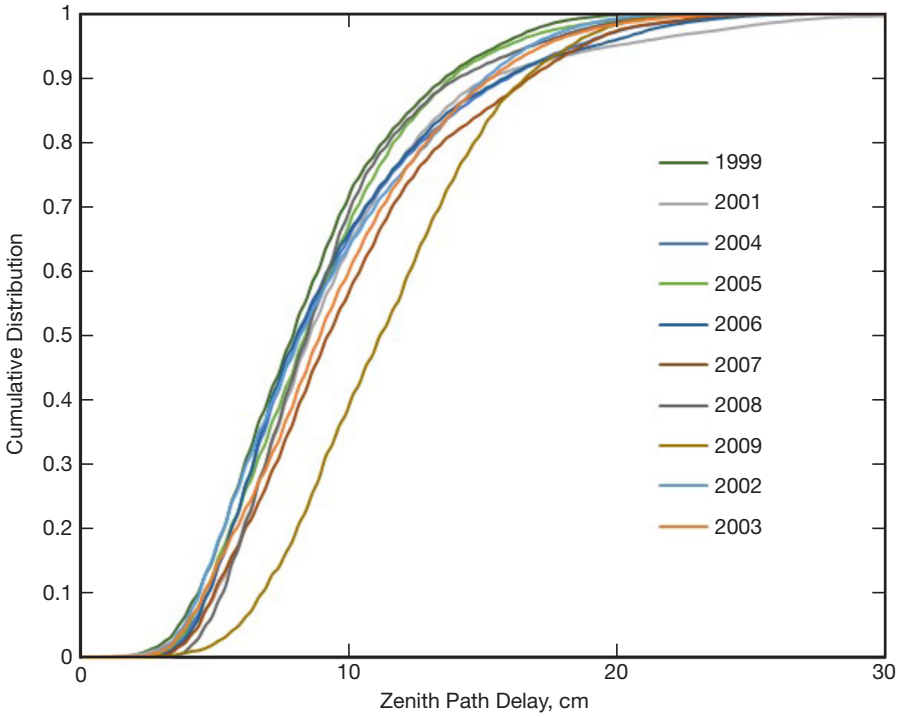


**Figure 11. Cumulative distribution of zenith wet path delay for Canberra.**

**Table 9. Zenith wet path delay statistics, Canberra WVR.**

| Year | Number of Data Points | Average, cm | Minimum, cm | Maximum, cm | 50% CD, cm | 90% CD, cm | 99% CD, cm | 99.9% CD, cm |
|---|---|---|---|---|---|---|---|---|
| 1999 | 51065 | 8.53 | 1.10 | 23.00 | 7.88 | 13.38 | 18.13 | 20.38 |
| 2001 | 60400 | 9.78 | 1.00 | 41.60 | 8.38 | 15.13 | 26.88 | 36.63 |
| 2002 | 102435 | 9.17 | 1.70 | 31.70 | 8.13 | 14.88 | 19.63 | 22.13 |
| 2003 | 97444 | 9.62 | 2.00 | 29.80 | 8.88 | 15.13 | 21.13 | 24.88 |
| 2004 | 77362 | 9.42 | 2.10 | 29.50 | 7.88 | 15.88 | 22.63 | 25.88 |
| 2005 | 69445 | 8.98 | 2.10 | 31.70 | 8.38 | 13.63 | 19.88 | 25.38 |
| 2006 | 102865 | 9.39 | 2.00 | 33.20 | 7.88 | 15.63 | 23.38 | 26.63 |
| 2007 | 67419 | 10.16 | 1.00 | 42.10 | 9.13 | 16.63 | 22.38 | 24.88 |
| 2008 | 43725 | 9.20 | 3.00 | 27.80 | 8.38 | 13.88 | 20.38 | 24.13 |
| 2009 | 21409 | 11.54 | 2.50 | 28.50 | 11.13 | 16.38 | 20.38 | 22.88 |
| Overall | 693569 | 9.58 | 1.00 | 42.10 | 8.60 | 15.05 | 21.48 | 25.38 |

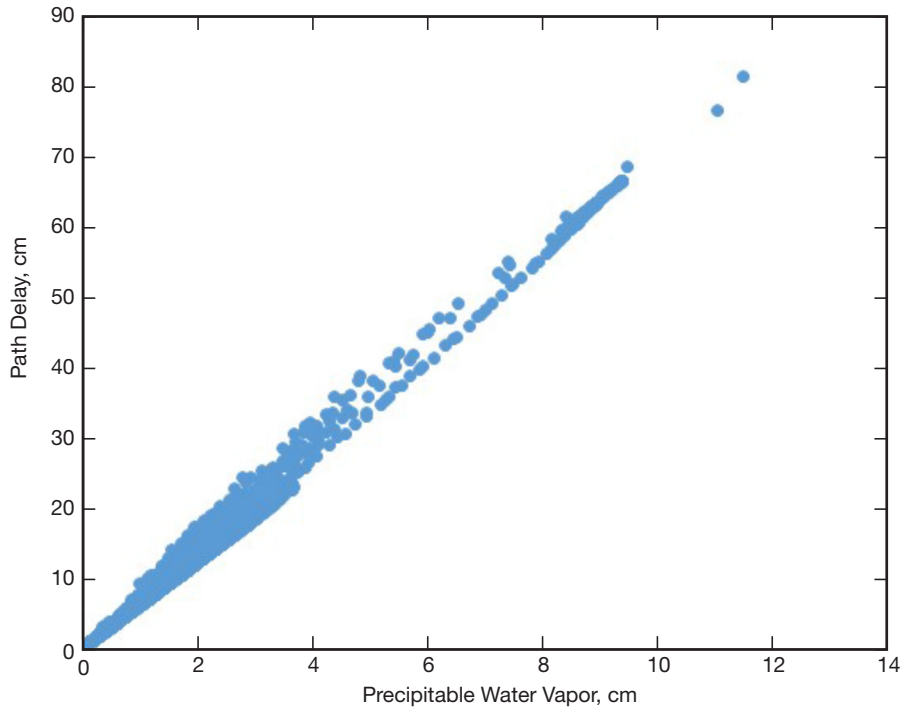


**Figure 12. Goldstone path delay versus precipitable water vapor along zenith for year 2004.**

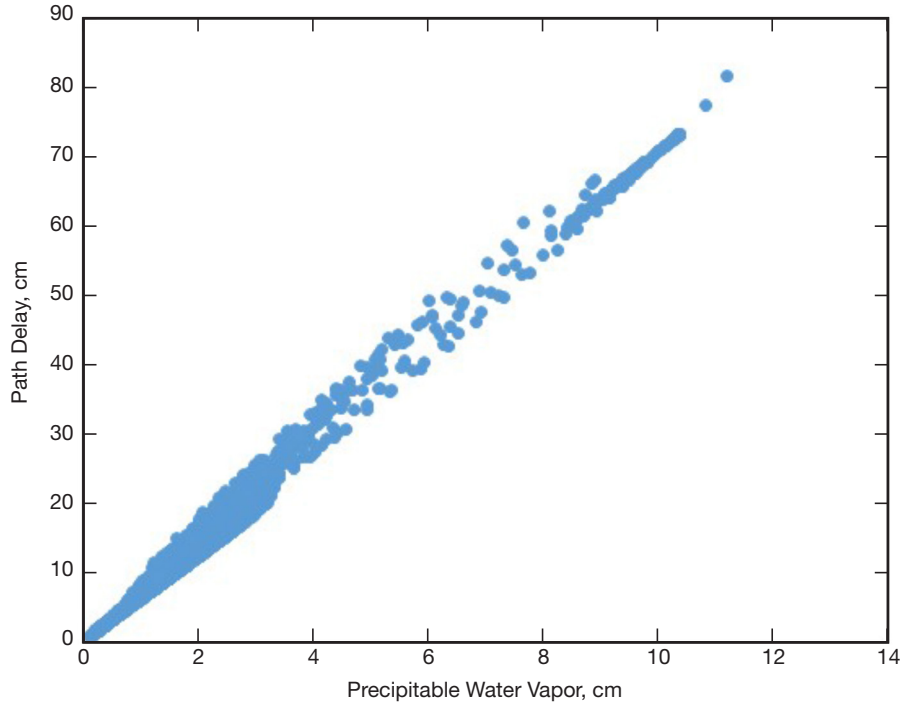


**Figure 13. Madrid path delay versus precipitable water vapor along zenith for year 2009.**

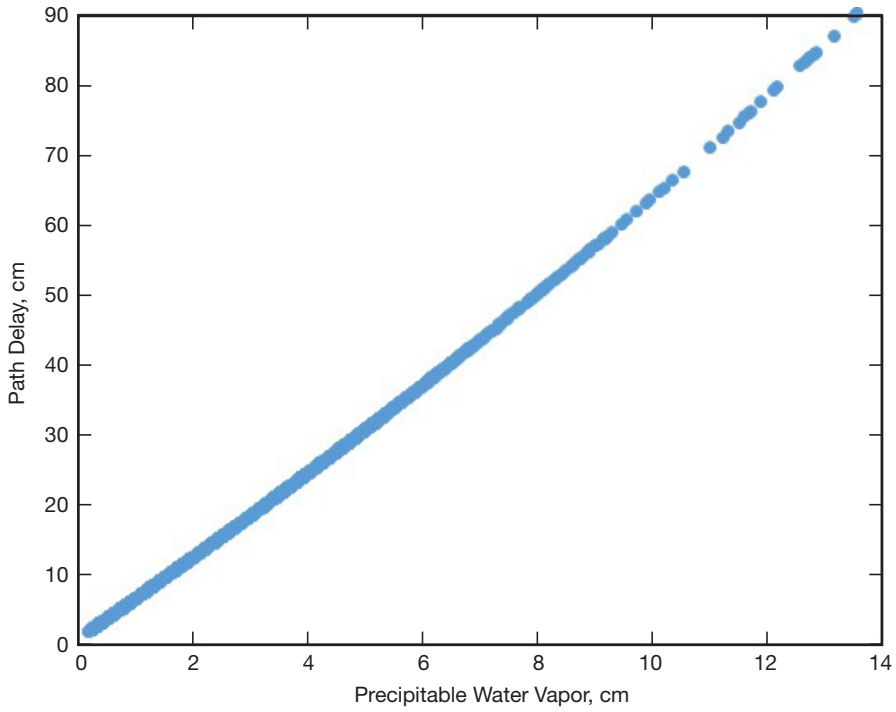


**Figure 14. Canberra path delay versus precipitable water vapor along zenith for year 2006.**

The Goldstone (6.51) and Madrid (6.65) AWVR-derived slopes are in good agreement with that (6.48) cited in [2], which was derived given a temperature of 281.65 K. The Canberra slope (6.00) does not exhibit as good agreement but it should be noted it was derived from the data from a much older model WVR (R06), which has a higher uncertainty. The reason that the Canberra data in Figure 14 have no apparent scatter is that a quadratic fit was used to directly convert the retrieved PD values to Vz [15]. This was done since there was no longer access to radiosonde data in Canberra that were used to produce the original path delay and liquid water algorithms. The quadratic fits were derived from ~20 island radiosonde site data sets and stem from the fact that the path delay has a small temperature dependence, second-order to the vapor density profile dependence (higher temperatures allow for higher vapor densities). Quadratic fits should provide a better fit to the path delay versus precipitable water vapor data. However, the scatter seen in the Goldstone and Madrid AWVR-based results in Figures 12 and 13, respectively, do not warrant performing second-order fits for these sites.

## VI. Conclusions and Other Studies That Will Make Use of the AWVR Data Sets

The current study examines the statistics of columnar water vapor, columnar liquid, and path delay extracted from WVR data using several calibration and inversion algorithms. The study on columnar water vapor compared this quantity derived from WVR data sets to that from ITU global maps. The result was that the WVR and ITU curves were in reasonable agreement with some discrepancies (primarily at Goldstone). Comparisons were also performed for columnar liquid and wet path delay. These data sets will also be used for examining time series correlations of path delay and liquid water content with other data

sources such as phase statistics or rain gauge data, respectively. Future work includes making use of these WVR-derived meteorological statistics in weather forecasting studies applicable for future Ka-band operational scenarios.


## Acknowledgments

We thank Kar-Ming Cheung and Faramaz Davarian for providing support for this work, Connie Dang of Exelis for providing DSN weather data support, and Bruce MacNeal for developing software tools used in some of the data processing. We are especially grateful to Harvey Berger of Northrop-Grumman, whose comments and contributions were very important from an ITU perspective.


## References


[1] S. D. Slobin, "Atmospheric and Environmental Effects," *DSN Telecommunications Link Design Handbook*, DSN No. 810-005, Space Link Interfaces, Module 105, Rev. E, Jet Propulsion Laboratory, Pasadena, California, issue date October 22, 2015. http://deepspace.jpl.nasa.gov/dsndocs/810-005/105/105E.pdf

[2] W. L. Flock, S. D. Slobin, and E. K. Smith, "Propagation Effects of Radio Range and Noise in Earth–Space Telecommunications," *Radio Science*, vol. 17, no. 6, pp. 1411–1424, November–December 1982.

[3] B. Bertotti, L. Iess, and P. Tortora, "A Test of General Relativity Using Radio Links with the Cassini Spacecraft," *Nature*, vol. 425, no. 6956, pp. 374–376, September 25, 2003.

[4] R. P. Linfield, L. P. Teitelbaum, L. J. Skjerve, S. J. Keihm, S. J. Walter, M. J. Mahoney, and R. N. Treuhaft, "A Test of Water Vapor Radiometer–Based Troposphere Calibration Using VLBI Observations on a 21-Kilometer Baseline," *The Telecommunications and Data Acquisition Progress Report*, vol. 42-122, Jet Propulsion Laboratory, Pasadena, California, pp. 12–31, April–June 1995, article dated August 15, 1995. http://ipnpr.jpl.nasa.gov/progress_report/42-122/122I.pdf

[5] G. Elgered, "Tropospheric Radio Path Delay From Ground-Based Microwave Radiometry," Chapter 5, *Atmospheric Remote Sensing by Microwave Radiometry*, edited by M. Janssen, New York: Wiley & Sons, 1993.

[6] D. D. Morabito, L. R. D'Addario, R. J. Acosta, and J. A. Nessel, "Tropospheric Delay Statistics Measured by Two Site Test Interferometers at Goldstone, California," *Radio Science,* vol. 48, 2013, doi:10.1002/2013RS005268. http://onlinelibrary.wiley.com/doi/10.1002/2013RS005268/abstract

[7] D. D. Morabito, L. R. D'Addario, S. Keihm, and S. Shambayati, "Comparison of Dual Water Vapor Radiometer Differenced Path Delay Fluctuations and Site Test Interferometer Phase Delay Fluctuations Over a Shared 250-Meter Baseline," *The Interplanetary Network Progress Report*, vol. 42-188, Jet Propulsion Laboratory, Pasadena, California, pp. 1–21, February 15, 2012. http://ipnpr.jpl.nasa.gov/progress_report/42-188/188A.pdf

[8] D. D. Morabito, "A Comparison of Estimates of Atmospheric Effects on Signal Propagation Using ITU Models: Initial Study Results," *The Interplanetary Network Progress Report*, vol. 42-199, Jet Propulsion Laboratory, Pasadena, California, pp. 1–24, November 15, 2014.
http://ipnpr.jpl.nasa.gov/progress_report/42-199/199D.pdf

[9] G. M. Resch, M. C. Chavez, N. I. Yamane, K. M. Barbier, and R. C. Chandlee, *Water Vapor Radiometry Research and Development Phase Final Report*, JPL Publication 85-14, Jet Propulsion Laboratory, Pasadena, California, April 1985.

[10] International Telecommunication Union, "Water Vapour: Surface Density and Total Columnar Content," Recommendation ITU-R P.836-3, Electronic Publication, Geneva, Switzerland, November 2001.

[11] International Telecommunication Union, "Attenuation due to Clouds and Fog," Recommendation ITU-R P.840-6, Electronic Publication, Geneva, Switzerland, 2013.

[12] S. J. Keihm, "Water Vapor Radiometer Measurements of the Tropospheric Delay Fluctuations at Goldstone Over a Full Year," *The Telecommunications and Data Acquisition Progress Report*, vol. 42-122, April–June 1995, pp. 1–11, August 15, 1995.
http://ipnpr.jpl.nasa.gov/progress_report/42-122/122J.pdf

[13] International Telecommunication Union, "Effects of Tropospheric Refraction on Radio Wave Propagation," Recommendation ITU-R P.834-6, Electronic Publication, Geneva, Switzerland, 2009.

[14] A. L. Berman and S. D. Slobin, "Tropospheric Path Length Fluctuation in Temperate Semiarid Locales: Application to the Gravitational Wave Experiment," *The Deep Space Network Progress Report*, vol. 42-55, Jet Propulsion Laboratory, Pasadena, California, November–December, 1979, February 15, 1980.
http://ipnpr.jpl.nasa.gov/progress_report2/42-55/55L.PDF

[15] S. J. Keihm, M. A. Janssen, and C. S. Ruf, "TOPEX/Poseidon Microwave Radiometer (TMR): III. Wet Troposphere Range Correction Algorithm and Pre-Launch Error Budget," *IEEE Transactions on Geoscience and Remote Sensing*, vol. 33, no. 1, January 1995.